

LETTER • OPEN ACCESS

## Identifying vulnerability factors associated with heatwave mortality: a spatial statistical analysis across Europe

To cite this article: B Sestito *et al* 2025 *Environ. Res. Lett.* **20** 044025

View the [article online](#) for updates and enhancements.

### You may also like

- [Social inequalities in exposure to heat stress and related adaptive capacity: a systematic review](#)  
S Claire Slesinski, Franziska Matthies-Wiesler, Susanne Breitner-Busch et al.
- [Exploring vulnerability to heat and cold across urban and rural populations in Switzerland](#)  
Evan de Schrijver, Dominic Royé, Antonio Gasparrini et al.
- [Impacts of climate change on groundwater quality: a systematic literature review of analytical models and machine learning techniques](#)  
Tahmida Naher Chowdhury, Ashenafi Battamo, Rajat Nag et al.

ENVIRONMENTAL RESEARCH  
LETTERS

## LETTER

## OPEN ACCESS

RECEIVED  
1 August 2024REVISED  
18 December 2024ACCEPTED FOR PUBLICATION  
5 March 2025PUBLISHED  
21 March 2025

Original Content from  
this work may be used  
under the terms of the  
[Creative Commons  
Attribution 4.0 licence](#).

Any further distribution  
of this work must  
maintain attribution to  
the author(s) and the title  
of the work, journal  
citation and DOI.



## Identifying vulnerability factors associated with heatwave mortality: a spatial statistical analysis across Europe

B Sestito<sup>\*</sup> , L Reimann<sup>\*</sup> , M Mazzoleni, W J W Botzen and J C J H Aerts

Institute for Environmental Studies, Vrije Universiteit Amsterdam, Amsterdam, The Netherlands

<sup>\*</sup> Author to whom any correspondence should be addressed.E-mail: [b.sestito@vu.nl](mailto:b.sestito@vu.nl)**Keywords:** heatwaves, social vulnerability, heat vulnerability index, heatwave mortality, extreme heat, heat stress, vulnerability driver

## Abstract

In recent decades, Europe has experienced severe heatwaves with significant mortality impacts. While hazard and exposure are key factors, vulnerability drivers play a crucial role in shaping these outcomes. However, few studies have examined these drivers at a continental scale. This study presents the first dynamic heat vulnerability assessment for Europe, incorporating spatial and temporal dimensions through ordinary least squares regression. Subnational (NUTS2) heatwave mortality data is used as the dependent variable, while independent variables include high-resolution raster data on heat hazard parameters, estimated population exposure, and socio-economic, demographic, and environmental vulnerability factors at both raster and subnational (NUTS2) scales. Our results (adjusted  $R^2 = 0.662$ ) identify foreign citizenship and urbanization as the most influential drivers, with a 1% increase in the percentage of foreign citizens and the size of urban areas associated with a 12.1% and 7.3% rise in heatwave-related mortality, respectively. Based on these findings, we construct the European heat vulnerability index for 2000–2019 as a weighted sum of the identified drivers, using the regression coefficients as weights. The results suggest that foreign citizens may face increased heat vulnerability due to intersecting socioeconomic factors. Policy recommendations include promoting inclusive integration measures to address disparities among foreign populations, and prioritizing sustainable urban planning and nature-based solutions to enhance resilience in rapidly urbanizing areas, ensuring equitable access to green spaces.

## 1. Introduction

Heatwaves can have a substantial impact on human health [1], causing, for example, dehydration, increased blood viscosity, and alteration of heart functions, such as heart rate, cardiac output, and arterial pressure [2], ultimately leading to cardiac failure [3, 4]. Numerous studies have shown a correlation between the occurrence of heatwaves and increased morbidity (defined as the state of being unhealthy because of a particular disease or condition) and mortality (defined as the number of deaths that occur in a population) [3, 5–9]. For example, the 2003 summer heatwave that hit Western Europe caused over 70 000 deaths [10]. Since climate change is expected to increase the frequency and intensity of heatwaves [11], the associated impacts are likely to rise as well. Risk frameworks and vulnerability

assessments play a crucial role in predicting heatwave impacts, especially in identifying high-risk areas and informing adaptation strategies [12]. Vulnerability, a key component of risk, is challenging to quantify because it encompasses the propensity of communities to suffer harm across various dimensions and because it includes physical, economic, and social factors [11]. These factors can vary significantly when assessing vulnerability to different hazards [13]. To enhance our understanding of heatwave risk in Europe, it is essential to identify which factors influence heat vulnerability and to what extent, as well as to establish the locations of vulnerable populations [14, 15]. The literature evidences the correlations between demographic, socioeconomic, and built environment variables and the effects of heatwaves. Our study's framework is similarly grounded on this selection:

- 1. Demographic factors such as age are critical to heat vulnerability. Elderly individuals (65+) are at heightened risk due to physiological declines in thermoregulation and the prevalence of chronic conditions [16, 17], while children under five are particularly susceptible due to their underdeveloped thermoregulatory systems and dependency on caregivers [18, 19].
- 2. Socioeconomic factors shape vulnerability by influencing access to adaptive resources and awareness of heat risks. Low income and education levels are associated with reduced capacity to cope with heat [3, 20]. Limited income gives individuals less access to household amenities such as air conditioning, fans, and proper ventilation systems that can help reduce the impacts of heatwaves [21]. Low education is linked to a lack of awareness regarding precautionary measures and potential dangers of heat [22, 23]. Economic insecurity and systemic inequities, reflected in unemployment and racial or ethnic disparities, can amplify risks. Contributing factors include limited access to resources, cultural differences, and the ongoing social, economic, and political marginalization linked to foreign descent or diverse backgrounds [24, 25]. Accessibility to healthcare also influences heat outcomes, encompassing both social and built environment dimensions. Socially, healthcare access depends on the affordability and functionality of health systems, which vary in their capacity to meet population needs. Physically, the proximity of healthcare facilities impacts timely medical intervention during heat-related emergencies [16].
- 3. Characteristics of the built environment such as urbanization amplify heat exposure through the urban heat island (UHI) effect, which increases temperatures in densely built-up areas compared to rural surroundings [26]. The lack of green spaces in urban environments exacerbates the issue by reducing opportunities for cooling. Recently, this problem has been examined through the lens of climate justice, which seeks to ensure equity and fairness in addressing climate change challenges, and some have advocated for the protection of the most vulnerable individuals, ensuring they are not disproportionately affected by climate change impacts [27]. Numerous case studies indicate that green spaces in urban areas are not only lacking but are also unequally distributed, leaving vulnerable, lower-income suburban areas disproportionately subject to heat stress within the urban environment [28–32]. Additionally, urban areas present further challenges because of their high reliance on public transportation and non-motorized modes of transport, which increases heat exposure, particularly for individuals with low socioeconomic status [33].

Despite existing research into vulnerability factors and heatwave risk, several challenges remain.

First, vulnerability factors vary over time and space. For example, a community's vulnerability can change significantly because of shifts in socioeconomic and demographic factors, such as population growth or decline, income level changes, urban development, and modifications to social infrastructure [34]. These temporal dynamics in vulnerability assessments have been rarely included in vulnerability studies [35].

Second, most studies on vulnerability and heat risk are locally-focused on cities or regions [20, 36–38], with few having a national spatial scope while using sub-national spatial units of analysis, such as studies conducted in the Netherlands [39] and South Korea [40]. Rohat *et al* [15] broadened the scope by conducting a continental vulnerability and heat risk assessment for Europe, considering a range of climate change and socioeconomic scenarios. However, their study relied on a definition of heatwave that does not include humidity, and their method was not validated against impact metrics. Chambers [41] offer a global analysis of heat vulnerability with national spatial scale.

Third, composite vulnerability indices are rarely validated against impact data, despite the importance of such validation to bridge the gap between theoretical evaluations and real-world consequences [42]. Some studies have undertaken this validation process using impact metrics—such as mortality [43], built environment damage [44], economic losses [45], or human migration [46]. In research related to heat, notable examples are predominantly found in the United States, originating from the work of Reid *et al* [47], who validated the heat vulnerability index (HVI) through regression analyses with morbidity or mortality data. Outside the US, such validation efforts are scarce and largely confined to local case studies, with limited exploration of applications with a regional or larger spatial scope [42, 48].

By addressing these challenges, this study aims to develop a dynamic HVI for Europe that better captures the evolving nature of heat vulnerability across regions and time periods [34]. Through its novel methodology, the study identifies key drivers of heat vulnerability among demographic, socioeconomic, and built environment variables by quantifying their statistical relationship with heatwave-related mortality data. In doing so, the study seeks to balance the complexity of vulnerability factors, which often encompass multiple interconnected dimensions, with the practical need to focus on the most informative indicators. By identifying these key determinants and ensuring they are statistically robust and not overly correlated, the analysis builds a data-driven, weighted index. The resulting tool provides a robust means for

assessing the spatial and temporal dynamics of vulnerability from 2000 to 2019, offering critical insights for evidence-based adaptation strategies.

## 2. Methodology

The methodology proposed in this study is summarized in figure 1. We identified impact, hazard, exposure, and vulnerability data to develop the European HVI (Eu-HVI). Impact data is represented by the number of fatalities associated with heatwaves (section 2.1). In the hazard data analysis, we processed atmospheric variables in order to derive heatwave footprints (section 2.2). Exposure was measured by the computed average exposed population in the heatwave footprint (section 2.3). Socio-economic and demographic variables such as age, education, GDP, foreign citizenship, and urbanization were used to determine vulnerability (section 2.4). As described in section 2.5, a regression analysis was applied to assess the key drivers of heat mortality. The most relevant drivers were used to calculate the Eu-HVI.

### 2.1. Impact

To understand the methodology of this study, we first describe the dataset on heatwave-related fatalities, sourced from the Risk Data Hub [49], which relies on the EM-DAT database [50]. The dataset records fatalities attributed to individual summer heatwave events (June to August) and compiles data from diverse sources, including governmental reports, international agencies, and press articles. It is available at two levels of nomenclature of territorial units for statistics (NUTSs): NUTS2 (intermediate-level regions) and NUTS3 (smaller regions). For this study, we used NUTS2 data (2021 classification) to align with the availability of vulnerability variables. Only heatwave events from 2000–2019 were included due to limited data availability prior to 2000.

### 2.2. Hazard

After impact, the second key component of this study's methodology is hazard. To delineate the hazard component, we employed the pan-European heatwave definition established by the EuroHEAT project [51]. Following this method, heatwaves are defined as periods of at least two consecutive days with a daily maximum apparent temperature  $T_{app-max}$  exceeding the 90th percentile of the monthly distribution (refer to appendix A for details on the computation of the  $T_{app}$  90th percentiles). The apparent temperature  $T_{app}$  is calculated as in equation (1) [51],

$$T_{app} = -2.653 + 0.994 * (T_{air}) + 0.0153 * (T_{dp})^2. \quad (1)$$

Here,  $T_{app}$  is a function of the surface air temperature  $T_{air}$  and the surface dew point temperature  $T_{dp}$ .  $T_{dp}$  is the temperature to which surface air would have to be cooled for saturation to occur; it is a measure of air moisture. The combination of high heat and humidity is a measure of human relative discomfort, as derived from physiological studies on evaporative skin cooling [52]. Calculating the heatwave footprints for past events associated with reported fatalities is essential for retrieving key event characteristics, including intensity, duration, and spatial extent, which are necessary for estimating the population exposed to the event. Starting with hourly data, we derive regional estimates of the temperature ( $T$ ) and duration ( $N$ ) of the heatwave. Visual examples of the variables  $T$  and  $N$  for selected events are shown in the methodology flowchart (figure 1). As an additional hazard metric, we include regional averages of land surface temperature (LST) to characterize differences in heat retention due to varying urban spatial structures and the UHI effect, as extensively documented in the literature (e.g. [53–55]). The LST data are obtained from the European Space Agency LST\_cci satellite observations dataset [56], with daily records in day and night-time and a spatial resolution of 1 km. Detailed steps of the calculation of the heatwave footprints and LST parameters are provided in appendix A.

### 2.3. Exposure

The third key component of this study's methodology is exposure. To assess population exposed to heatwaves, we combine the gridded heatwave footprints (section 2.2) with raster population data from GHS-POP [57], at a 30 arc seconds spatial resolution. Since the time span of this study is 2000–2019, we use the available population data from 2000, 2005, 2010, 2015 and 2020. The population data for the intermediate years is computed by applying the yearly growth rate extrapolated from the reference years [58]. To calculate the average population exposed to the heatwave events, we overlay the heatwave footprint mask with the population raster, filtering out individuals not located within the heatwave-affected areas. Similar to the hazard components, we then aggregate all the individuals exposed to heatwaves falling within the same NUTS2 region and average them throughout all days of the heatwave duration.

### 2.4. Vulnerability

The final step in data processing focused on selecting and preparing vulnerability variables for the regression analysis. These variables were chosen based on existing literature while ensuring compatibility with the constraints of pan-European data availability, subnational granularity, and sufficient temporal coverage. A detailed overview of the vulnerability

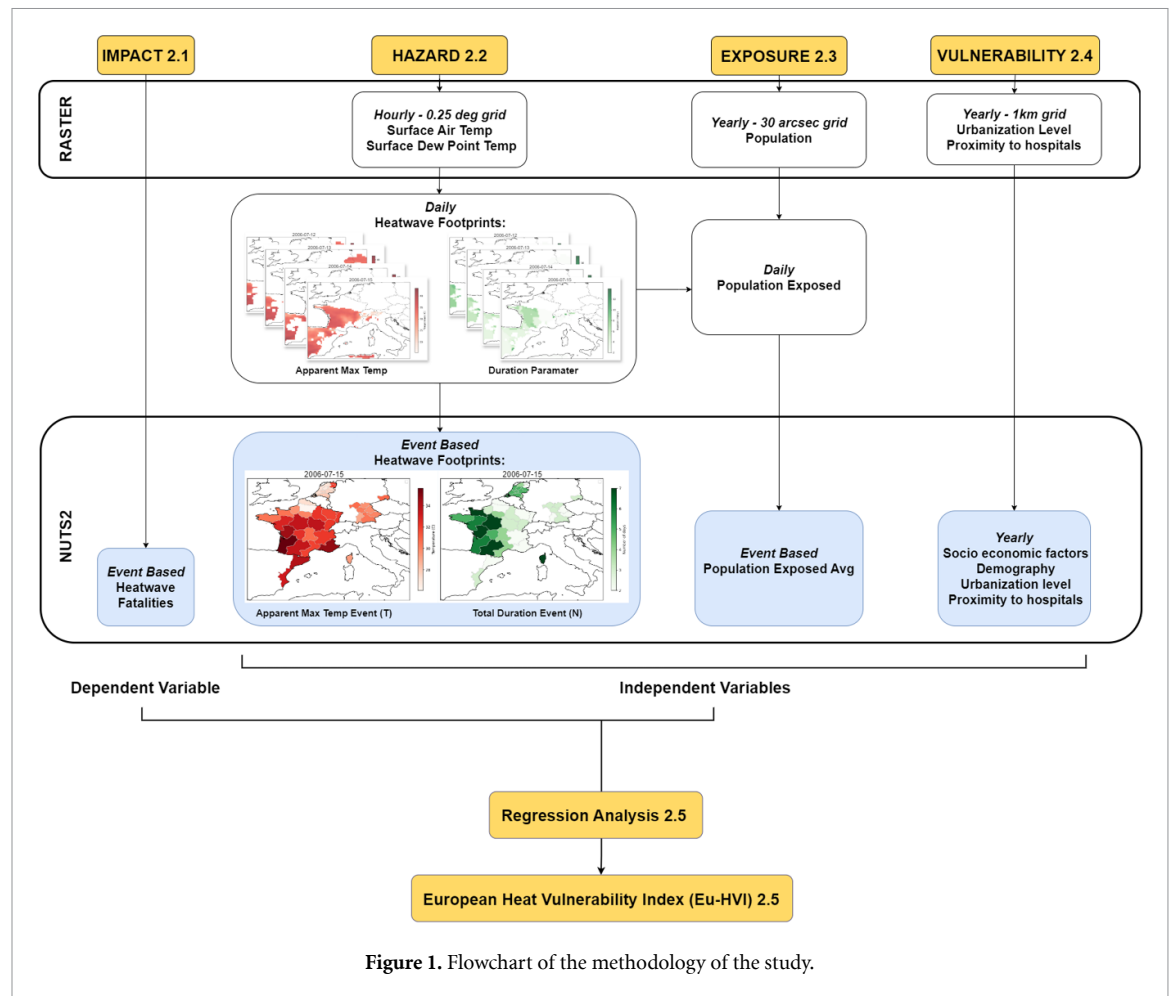


Figure 1. Flowchart of the methodology of the study.

variables, alongside the impact, hazard, and exposure components used in the statistical analyses, is provided in table 1.

The vulnerability variables included in this study are derived from the literature, as described in the introduction, and consist of factors such as age (elderly and children), socioeconomic status (income, education, unemployment), percentage of foreign citizens, national adaptive capacity, healthcare access, and urbanization. While the inclusion of many of these variables is self-explanatory, a few require additional clarification to justify their relevance in this context.

In particular, the percentage of foreign citizens was used as a vulnerability determinant due to the lack of consistent data on race or ethnicity. This variable is intended to capture potential disadvantages faced by foreign populations, which may be subject to higher vulnerability due to socio-economic inequalities and integration challenges in host countries.

Healthcare access is another critical factor, measured by the distance to hospital facilities as a proxy for physical accessibility. This reflects the ability to access preventive and emergency medical care, especially in countries with socialized healthcare systems. However, it should be noted that this measure does

not encompass the broader social aspects of healthcare access, such as insurance affordability or the privatization of healthcare services.

The Notre Dame Global Adaptation Initiative's (ND-GAIN) Country Index [59] was also tested as a proxy for national-level adaptive capacity to climate change, providing an additional layer of insight into vulnerability at the country level.

While the UHI effect is incorporated into the hazard component of the analysis, the degree of urbanization was also considered as a vulnerability determinant. Urban areas tend to amplify heat stress due to the concentration of people, limited green spaces, and greater reliance on public transportation, which increases exposure for vulnerable groups [30, 33]. Since this study focuses on heat vulnerability at the NUTS2 level across Europe, it cannot fully capture intra-city inequalities. To address this, categorical variables reflecting varying levels of urbanization were introduced. The GHS-SMOD [60] raster data was used to classify 1 km × 1 km grid cells based on settlement types, categorizing regions into *Urban Centre* (cities), *Urban Cluster* (dense/semi-dense towns and sub/peri-urban areas), and *Rural* (villages, dispersed rural, or predominantly uninhabited areas).

**Table 1.** Specifications of the variables adopted in this study. The *Proxy variables* column lists the processed variables used as independent variables in the regression analysis (section 2.5). The source data are processed to obtain event specific values (Hazard and estimated average exposed population) or yearly values (Vulnerability) for each NUTS2 region.

Determinant	Proxy variables	Source	Source spatial resolution	Selected temporal resolution
Hazard				
Heatwave intensity	T (°C) (average of $T_{app-max}^{NUTS2}$ among the heatwave days)	[61]	0.25° (Global)	2000–2019 hourly
Heatwave duration	N (days)	[61]	0.25° (Global)	2000–2019 hourly
Urban heat island effect	LST (°C)—NUTS2 average among the heatwave days	[56]	1 km (Global)	2000–2019 daily
Exposure				
Estimated average exposed population	# of people (mln) exposed to heatwaves	[57]	30 arcsec	2000–2020 5-yearly (yearly interpolated)
Vulnerability				
Elderly	% (1–100) of people over 65 yo	[62]	NUTS2 (Europe)	2000–2019 yearly
Children	% (1–100) of children younger than 5 yo	[63]	NUTS2 (Europe)	2000–2019 yearly
Income	GDP at current market prices (Purchase power standards) per inhabitant (kPPS)	[64] [65]	NUTS2 (Europe) ITL2 (UK)	2000–2019 yearly 2000–2019 yearly
Education	% (1–100) of people with educational attainment level: a) Basic (less than primary, primary, lower secondary education) b) Intermediate (upper secondary and post-secondary non-tertiary education) c) Advanced (tertiary education)	[66]	NUTS2 (Europe)	2000–2019 yearly
Unemployment	% (1–100) of unemployed residents (from 15 to 74 years old)	[67]	NUTS2 (Europe)	2000–2019 yearly
Foreign citizens	% (1–100) of residents with foreign citizenship (from 15 to 74 years old)	[67]	NUTS2 (Europe)	2000–2019 yearly
Adaptive capacity	ND-GAIN country index	[59]	Country (Global)	2000–2019 yearly
Accessibility to healthcare	NUTS2 average motorized travel time to hospital facilities (minutes)	[68]	1 km (Global)	2019 (assumed constant)
Degree of urbanization	% (1–100) area of NUTS2 by settlement type: a) Urban center (High density cluster, >1500 inhabitants per km <sup>2</sup> and >50,000 inhabitants in the cluster) b) Urban cluster (Moderate density cluster, >300 inhabitants per km <sup>2</sup> and >5000 inhabitants in the cluster) c) Rural (<300 inhabitants per km <sup>2</sup> and/or not part of a cluster with sufficient population to be considered an urban cluster)	[60]	1 km (Global)	2000–2020 5-yearly (yearly interpolated)



## 2.5. Regression analysis and Eu-HVI

With the four components described in the previous sections, this study built on the methodology of Reimann *et al* [43] and utilized a multiple linear regression analysis to empirically derive a Eu-HVI at the continental scale for Europe, based on the dominant vulnerability factors in explaining heat mortality. We conducted an ordinary least squares (OLSs) regression with the heatwave fatalities ( $F$ ) as the dependent variable and the hazard ( $H$ ), exposure ( $E$ ), and vulnerability factors ( $V$ ) (table 1) as independent variables. To reduce the impact of outliers, we applied a log transformation to the heatwave fatalities data, as some events reported exceptionally high numbers [69]. Country dummy variables were included as independent variables to account for country-specific effects that we were not able to capture with the variables included, as elaborated in section 3. The heatwave fatalities of each event  $i$  are then modelled as equation (2),

$$\log(F_i) = \alpha + \beta_1^H H_{1,i} + \dots + \beta_3^H H_{3,i} + \beta^E E_i + \beta_1^V V_{1,i} + \dots + \beta_n^V V_{n,i} + \gamma_k C_{k,i}. \quad (2)$$

In this equation,  $\alpha$  represents the intercept of the model. The hazard variables are denoted as  $H_{1,i}, \dots, H_{3,i}$ , with corresponding coefficients  $\beta_1^H, \dots, \beta_3^H$ . The exposure variable  $E_i$  has an associated coefficient  $\beta^E$ . The vulnerability variables  $V_{1,i}, \dots, V_{n,i}$  are associated with coefficients  $\beta_1^V, \dots, \beta_n^V$ . Country-specific effects are captured by the dummy variable  $C_{k,i}$ , where  $C_{k,i} = 1$  if the  $i$ -th observation belongs to country  $k$ , and  $C_{k,i} = 0$  otherwise, with  $\gamma_k$  being the corresponding slope coefficient. The regression models were computed across all heatwave events in the dataset, incorporating variations across both time and space. The model estimates the intercept ( $\alpha$ ) and slope coefficients ( $\beta$  and  $\gamma_k$ ), which quantify the relationships between the independent variables and the dependent variable,  $\log(F_i)$ . For log-linear regression models, and when  $\beta$  values are small ( $<0.1$ ), each  $\beta$  can be interpreted as the approximate percentage change in  $F_i$  for a one-unit increase in the corresponding predictor, holding all other variables constant [70].

Our analysis explored various configurations of OLS models. The optimal model was selected through an automated algorithm developed by the authors that evaluates all possible combinations of independent variables, based on the ‘all possible regression’ approach [71]. The algorithm identified the most suitable models through the following methodology:

1. Input variable selection: independent variables were organized into three configurations:

- Configuration 1 ( $H + E$ ): hazard ( $H$ ) and exposure ( $E$ ).
- Configuration 2 ( $H + E + V$ ): hazard, exposure and vulnerability ( $V$ ).
- Configuration 3 ( $H + E + V + \text{dummies}$ ): hazard, exposure, vulnerability and country dummy variables.

2. Exhaustive combinations: for each configuration, the algorithm generated all possible variable sets based on the independent variables listed in table 1:

- Configuration 1 ( $H + E$ ):  $N_1 = 2^4 - 1 = 15$  combinations.
- Configuration 2 ( $H + E + V$ ):  $N_2 = 2^{17} - 1 = 131\,071$  combinations.
- Configuration 3 ( $H + E + V + \text{dummies}$ ):  $N_3 = 2^{18} - 1 = 262\,143$  combinations.

3. Multicollinearity: for each combination, the variance inflation factor (VIF) was calculated to assess multicollinearity. Only variable sets with  $VIF < 5$ , indicating low multicollinearity [72], were retained. This ensured minimal mutual correlation among the variables in the regression models.
4. OLS regression execution: OLSs regression with robust standard errors was conducted on the variable sets that passed the multicollinearity filtering.
5. Optimal model selection: models with adjusted  $R^2$  values in the 98th percentile of the distribution were shortlisted. Among these, the model with the highest number of statistically significant ( $p$ -value  $< 0.05$ ) independent variables was chosen as the optimal model. If multiple models met these criterion, the one with the highest adjusted  $R^2$  was selected.

This selection process ensured that the optimal model retained the maximum number of linearly independent explanatory variables while maintaining statistical robustness. To account for potential non-linearity in the data, robust standard errors were used in all regressions. The Akaike information criterion (AIC) was also tested as an alternative selection metric to adjusted  $R^2$ , yielding the same optimal model. To evaluate spatial autocorrelation, Moran's  $I$  test was applied to the residuals of the models [73]. As part of a sensitivity analysis, variables were individually added to or removed from the optimal model to assess the impact on its performance, the additional model configurations are provided in appendix C.

The Results section presents the optimal models for configurations 1, 2, and 3 (table 2).

The Eu-HVI (equation (3)) was calculated annually from 2000 to 2019 as a weighted sum of the

selected vulnerability variables  $V_j$ , with their slope coefficients  $\beta_j$  as weights [43, 74].

$$\text{Eu-HVI}_i = \sum_j^n \beta_j^V V_{j,i}. \quad (3)$$

We then aggregated the Eu-HVI at the NUTS2 level, and the resulting maps provided a visual representation of heat vulnerability across Europe. The Eu-HVI was linearly normalized to a range of 1–10 (with 1 indicating low and 10 high vulnerability), following other examples of vulnerability assessments [36, 43, 75]. The dynamics of heat vulnerability and its drivers can be assessed by analyzing temporal and spatial heterogeneous patterns.

### 3. Results

#### 3.1. Regression models

Table 2 presents the optimal models derived under the three configurations detailed in section 2.5. The first model, Model 1, represents the basic model, which reflects the optimal configuration when only hazard and exposure variables are provided as inputs to the algorithm. From this set, the algorithm selects ‘T’ (heatwave intensity) and ‘Pop Exp’ (population exposed) as the combination of explanatory variables that satisfy all conditions outlined in section 2.5.

Model 2 is generated when hazard, exposure, and vulnerability variables are included as inputs, excluding country dummy variables. Under this setup, the optimal model incorporates the percentage of urban center and urban cluster areas along with the percentage of foreign citizens, in addition to the hazard and exposure components.

Model 3 represents the optimal model when all variables—hazard, exposure, vulnerability, and country dummy variables—are included as inputs, allowing full flexibility in variable selection. In this configuration, no hazard variables appear in the final model, but the population exposed, the percentage of urban cluster areas and the percentage of foreign citizens are selected together with the country dummy variables. The following observations can be made from these results:

- The inclusion of vulnerability variables alongside hazard and exposure variables increases the explanatory power of the model by over 80%. This is evident from the rise in adjusted  $R^2$  from 0.201 in Model 1 to 0.375 in Model 2, coupled with a decrease in the mean absolute error.
- Adding country-specific dummy variables further doubles the explanatory power compared to Model 2, increasing  $R^2$  to 0.662 in Model 3. The mean absolute error also decreases significantly. In this configuration, hazard parameters are absent, implying that their contributions, along with country-specific effects not explained by the

other explanatory variables, are accounted for by the country dummy variables, which mitigates the omitted variables bias.

Additionally, all regression coefficients in the presented models are positive, indicating that a one-unit increase in each explanatory variable is associated with an increase in heatwave mortality. Given these findings, Model 3 is identified as the best-fit model, with 1% increase in urban cluster areas associated to 7.3% increase in heatwave mortality and 1% increase in residents holding foreign citizenship associated to 12.1% increase in heatwave mortality, and with a Morans’ I value of 0.3, which indicates minimal spatial structure, unlikely to bias the model results. Appendix B provides the correlation matrices and the VIF values for the selected models shown in table 2, as well as the correlation matrix of the full list shown in table 1.

#### 3.2. Eu-HVI

Using Model 3, the two vulnerability drivers (i.e. percentage of foreign citizens and urban cluster areas) and their coefficients were included as the components of the Eu-HVI (equation (3)). Figure 2 shows the Eu-HVI map, together with its components for the year 2019. The Eu-HVI (figure 2(a)) for 2019 reveals distinct regional heat vulnerability patterns across Europe, primarily influenced by its components: the percentage of foreign citizens (figure 2(b)) and urban cluster areas (figure 2(c)). Among these, the percentage of foreign citizens has a stronger influence, as indicated by its higher regression coefficient ( $\beta_{\text{for}} = 0.121$ ,  $\beta_{\text{urb}} = 0.073$ ). This combination results in prominent hotspots of heat vulnerability in Central Europe, particularly in the Benelux region, West Germany, Ile de France (Paris metropolitan area) and Switzerland. In Southern Europe, vulnerability exhibits spatial gradients driven by varying levels of urbanization and foreign citizens. For example, Northern Italy is more vulnerable than Southern Italy, while Eastern Spain displays higher vulnerability compared to the western Iberic Peninsula. Similarly, in the United Kingdom, vulnerability is high in the densely urbanized southern regions of the country. In contrast, Eastern Europe shows relatively homogeneous and low vulnerability scores within countries, reflecting its predominantly rural landscape and limited proportion of foreign citizens. Scandinavia and the Baltic region also exhibit generally low vulnerability, where rural areas dominate and the vulnerability patterns closely follow the distribution of foreign residents.

#### 3.3. Eu-HVI temporal dynamics

Figure 3 illustrates as an example the variation of the Eu-HVI and its components over the decade 2010–2019. The data reveal a notable increase in heat vulnerability across most of Europe, primarily



**Table 2.** Overview of the best-fit models achieved under three distinct configurations, with log(Fatalities) as dependent variable. Model 1 represents the optimal baseline model utilizing solely hazard and exposure as input independent variables. Model 2 is identified as the optimal model when the input independent variables include hazard, exposure, and vulnerability, with the exclusion of county dummies. Model 3 emerges as the optimal model when the model selection algorithm is provided with all available independent variables as input. The slope coefficients are reported with the robust standard error in brackets and their level of statistical significance (\*  $p < 0.05$ , \*\*  $p < 0.01$ , \*\*\*  $p < 0.001$ ).

Variables	Model 1 Baseline ( $H + E$ )	Model 2 No country dummies ( $H + E + V$ )	Model 3 Full flexibility ( $H + E + V + CD$ )
$H : T$ (deg C)	0.095*** (0.021)	0.162*** (0.021)	—
...	—	—	—
E: Pop Exp (mln)	0.365** (0.107)	0.166 (0.115)	0.285** (0.090)
V: %Urban cluster (1–100)		0.112*** (0.016)	0.073*** (0.017)
% Urban center (1–100)		0.014* (0.006)	—
%Foreign citizens (1–100)		0.074** (0.025)	0.121*** (0.027)
...		—	—
Country dummies (CD)			
AT			0.580 (0.860)
CH			0.948 (0.858)
CZ			2.133* (0.906)
DE			2.811*** (0.828)
EL			−0.037 (0.885)
FR			2.129* (0.910)
HU			3.935*** (0.911)
IT			−3.418 (1.984)
NL			2.702*** (0.831)
PT			2.507* (1.246)
UK			−0.088 (0.813)
Intercept	0.035 (0.558)	−2.888*** (0.573)	−0.005 (0.891)
N. Observations	278	251	251
Mean absolute error	1.411	1.117	0.727
Morans I	0.386**	0.437**	0.340**
AIC	1096	931	785
Adjusted R2	0.201	0.375	0.662

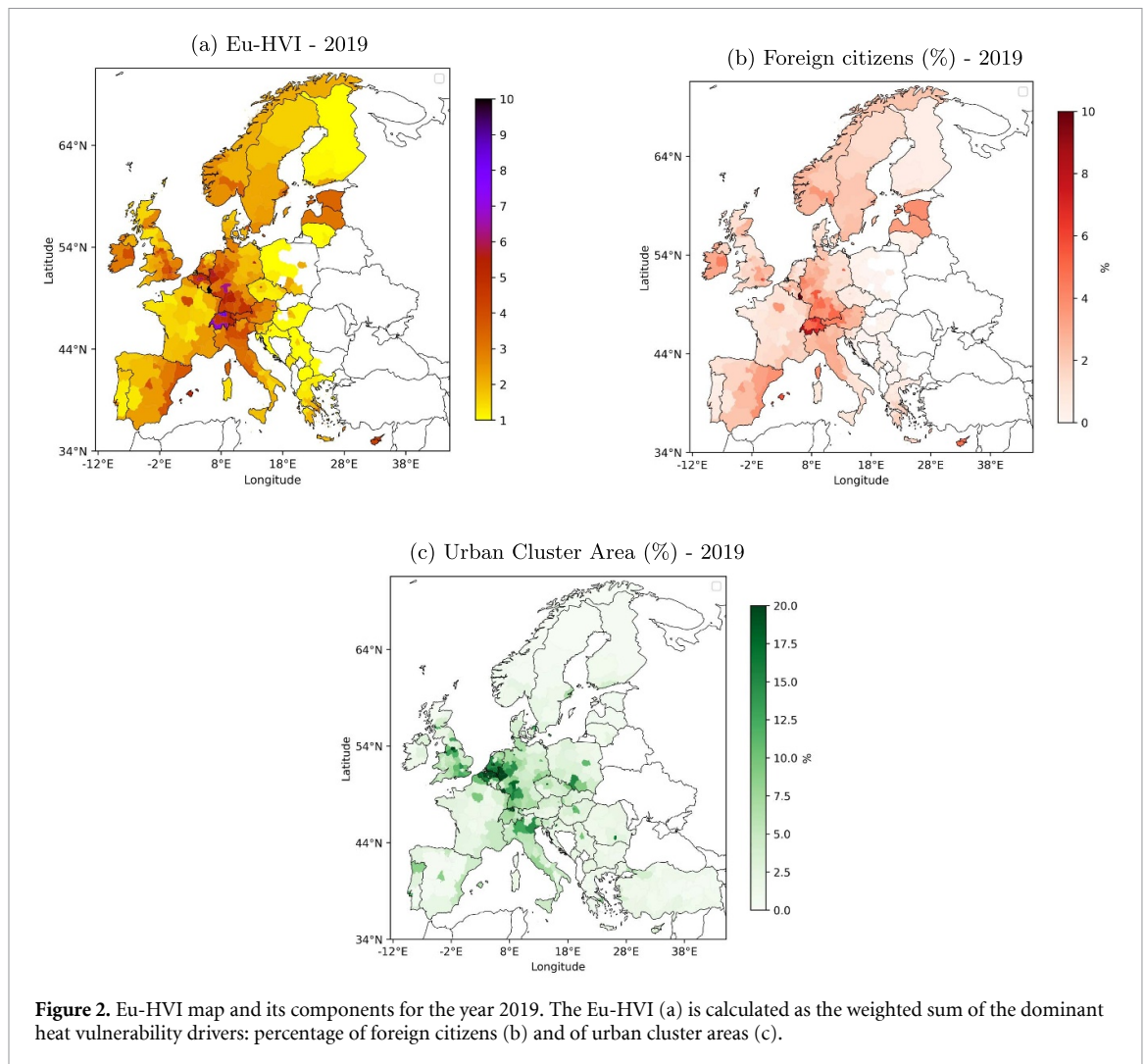
driven by the rising percentage of foreign citizens (figure 3(b)). This demographic change shows significant increases—exceeding +6% in some areas—with hotspots in Central Europe and widespread positive trends in Scandinavia, Germany, Italy, the UK, Austria, and much of France. In contrast, decreases in foreign citizenship percentages are observed in parts of the Iberian Peninsula, Greece, and the Baltic countries. The variation in urban clusters (figure 3(c)) is limited to a smaller range, typically within  $\pm 2\%$ , reflecting the slower pace of urbanization. However, it is noteworthy that in many areas where the percentage of urban clusters decreased, urban centers increased (figure 3(d)), thereby boosting overall urbanization.

## 4. Discussion

While this is the first dynamic HVI study for Europe validated on heat-related mortality data, our method and results lead to the following points for discussion: This study introduces a statistical method aimed at identifying the primary variables impacting heatwave-related mortality throughout Europe. When comparing Model 1 to Models 2 and 3, the higher exposure coefficient in Model 1 indicates that

incorporating vulnerability components in the subsequent models transfers a portion of the explanatory power from exposure to vulnerability. This transition facilitates a more refined comprehension of factors impacting heatwave mortality, while improving the models performances (i.e. higher  $R^2$ ). The baseline model (Model 1), depicting the effects of temperature and exposure, explains only a small portion of the variance in heatwave mortality. This underscores the necessity for ongoing investigations into the mechanisms of vulnerability in relation to heat-related mortality and highlights the value of integrating vulnerability components into heat risk assessments [11].

We identified the percentage of foreign citizens and the degree of urbanization, namely the percentage of urban clusters, as the primary heat vulnerability drivers. The finding that urban clusters are key determinants of heat vulnerability aligns well with existing literature. The connection between urban environments and heightened heat vulnerability is well documented [14, 36, 76, 77], highlighting that disadvantaged populations with lower socio-economic status often reside in areas with limited green spaces and higher heat exposure [28, 29, 78, 79]. The consistent identification of

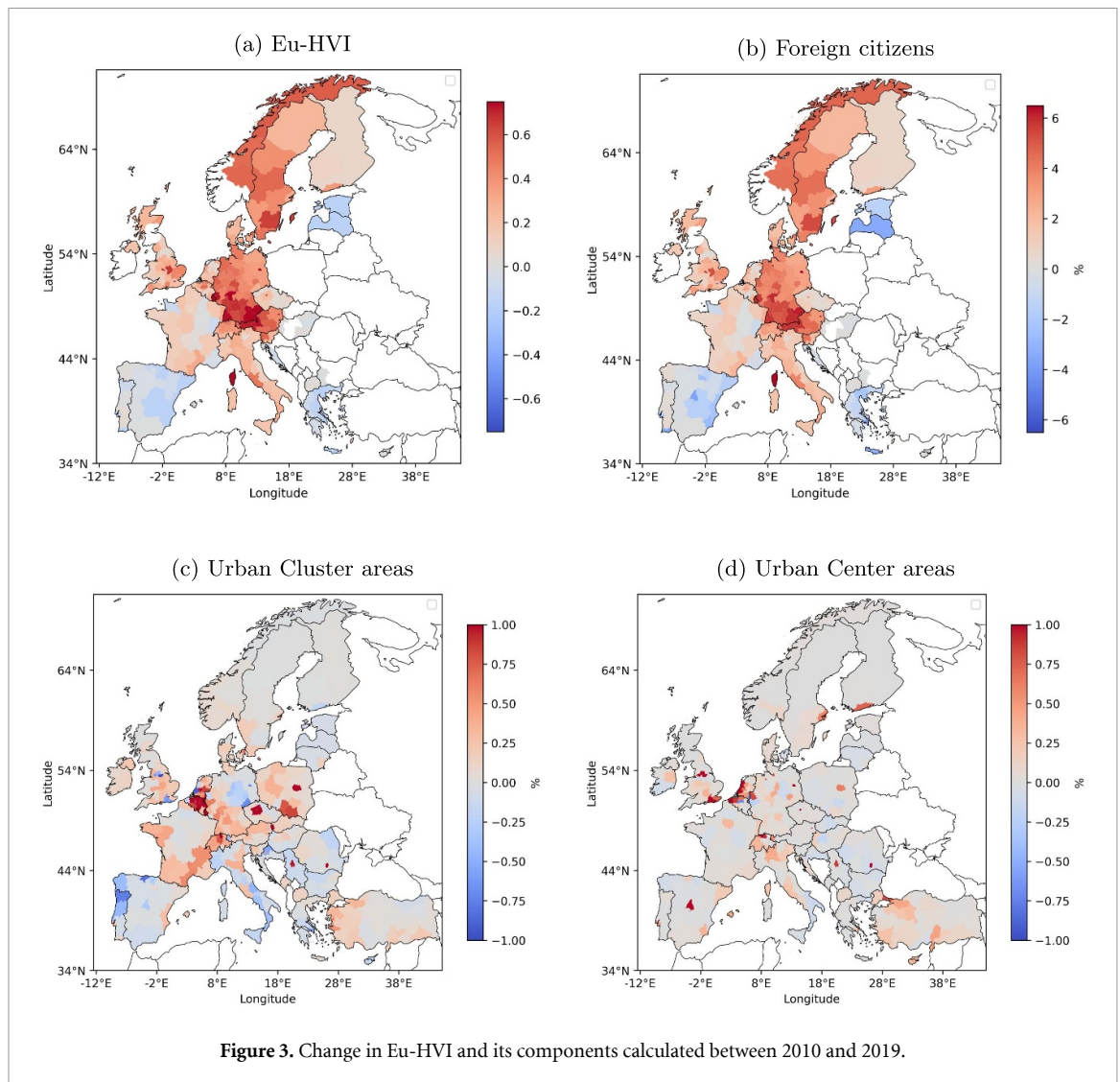


urbanization as a significant factor across diverse contexts underscores the need for urban-specific interventions, such as nature-based solutions, improved access to green spaces, and policies targeting environmental inequities. Future projections of ongoing urban expansion exacerbate the necessity of long-term strategies to mitigate urban heat vulnerability [80, 81].

The identification of foreign citizenship as a major driver of heat vulnerability introduces a less-explored dimension of heat impacts, particularly in the European context. Evidence from the United States demonstrates significant disparities among racial and ethnic minorities and foreign-born populations in climate change related health effects [82], and specifically in heat-related mortality and morbidity (e.g. [83–85]). Other studies report heightened risks for migrants and minority groups due to occupational exposure, lower socioeconomic status, and inadequate living conditions [86, 87]. Our findings suggest parallels in Europe, where foreign citizens may similarly face increased heat vulnerability due to intersecting factors such as lower socioeconomic status, language barriers, limited healthcare access,

precarious housing or working conditions. However, systematic investigations into racial or foreign status disparities on environmental and heat-related health in Europe remain scarce [88]. Furthermore, the use of foreign citizenship as a proxy for vulnerability requires careful interpretation. While this variable captures a critical dimension of heat risk, it may not fully encompass the nuances of immigrant experiences, such as race or ethnicity, cultural differences, time since migration, or occupational exposures. We suggest future research to expand on this dimension to include direct measures of socioeconomic and health disparities among immigrant populations.

A key aspect of this analysis is the application of country-specific dummy variables within regression models. This approach enhances the explanatory power of the optimal model by spotlighting shared vulnerability determinants across Europe while incorporating country-specific factors like climate conditions, cultural and behavioral aspects, varied thermal adaptability, healthcare quality, and national strategies for adaptation [89], along with heat action plans [90] which are not fully represented by the existing set of independent variables. The



inclusion of the ND-GAIN Adaptation country index was found to contribute minimally to model performance, resulting in an inadequate capture of significant country-specific effects (refer to appendix C). With the integration of country dummy variables, maximum temperature ( $T$ ) does not significantly predict outcomes in the optimal model. This suggests that incorporating country-specific factors filters out the inherent climatic characteristics of different nations. However, while country dummy variables offer insights into national-scale adaptation patterns, they do not account for intra-country variations. Sub-national regions, such as urban capitals or rural areas, may share socio-demographic characteristics that influence vulnerability across borders. Investigating these local-level drivers of vulnerability is an important area for future research.

While heat vulnerability drivers are often studied at the local scale, this analysis highlights the significance of continental-level determinants, specifically foreign citizenship and urbanization, which consistently demonstrate explanatory power across Europe. These factors reflect the intricate interplay

of socioeconomic and environmental conditions, underscoring the challenge of disentangling the multifaceted nature of vulnerability. While the index emphasizes the dominant, non-collinear factors, it does not capture all context-specific vulnerabilities. Nevertheless, it serves as a valuable tool for understanding the spatial and temporal patterns of the two primary continental-level components and their overlap. This broader perspective enhances our understanding of heatwave mortality across Europe and provides a solid foundation for developing targeted, evidence-based interventions. Such insights can guide strategies at multiple scales, from urban planning to continent-wide adaptation policies, fostering a more comprehensive response to heat vulnerability. Within this framework, it is essential for EU-level policies to incorporate nature-based solutions and sustainable urban planning [91, 92], aimed at optimizing urban greenery configurations [93] and addressing environmental inequities [94]. Additionally, policies need to address integration measures and carefully analyze inequalities associated with foreign status to guide

equitable climate adaptation strategies, in light of Europe's demographic changes.

While our study presents significant findings, it is important to acknowledge its limitations. One notable limitation is the spatial resolution of the source heatwave mortality and vulnerability data. The lack of consistent high-resolution impact data across Europe constrains this limitation. NUTS2 spatial aggregation does not allow for smaller-scale variations. One example is the relatively uniform spatial and temporal age distribution across the NUTS2 regions observed in the source data, compared to the dominant vulnerability drivers, which show more pronounced variations. This homogeneity limits our ability to capture age-related vulnerability differences. Moreover, the NUTS2 resolution is insufficient for examining intra-urban disparities and drawing comparisons between cities. To refine our methodology and achieve a more precise ranking of cities based on heat vulnerability, future research could repeat the analysis with high-resolution city-level vulnerability and impact data. This approach would allow for a deeper exploration of additional socio-economic factors contributing to heat vulnerability [13], which are at the core of climate injustice and social inequalities within urban areas. However, the availability of such high-resolution data is still a limiting factor [95]. An additional limitation observed in our regression analysis is the non-significance of LST, which was not included in the final models based on our selection criteria (see table 2). Any model configuration incorporating LST resulted in reduced performance. In contrast, the degree of urbanization consistently emerged as a dominant driver. We hypothesize that the NUTS2 spatial aggregation may not be sufficiently fine-grained to capture the physical UHI effect, making urbanization a more effective proxy at this scale. Additionally, urbanization may also encompass other contributing factors, such as social inequalities, which could explain the stronger association between urban areas and heatwave mortality. Moreover, our regression models presuppose linear dependencies between variables. However, this is an approximation due to the constraints of the dataset and our emphasis on a first-order analysis for straightforward interpretability. Future research should explore non-linear approaches with richer datasets to better capture complex interactions between vulnerability drivers and heatwave mortality.

## 5. Conclusions

This study presents the first spatiotemporal dynamic heat vulnerability assessment on a continental scale for Europe. Through regression analysis of heatwave mortality data, foreign citizenship and urbanization emerged as key vulnerability factors, with a 1% increase in these variables associated with 12.1%

and 7.3% rises in heatwave mortality, respectively. These findings underscore the importance of addressing shared transboundary drivers of vulnerability to develop effective, EU-wide strategies for reducing heat-related mortality.

As climate change intensifies heatwave frequency and severity [11] and urbanization is projected to grow [80], the need for equitable and sustainable solutions becomes increasingly urgent. Urban greening and sustainable spatial planning are essential for reducing UHI effects; however, it is crucial to implement these measures in ways that also address inequities in access to cooling and heat exposure. Future research should focus on unraveling the social inequalities linked to heat vulnerability in Europe, particularly by examining inter-urban vulnerabilities and the socio-economic and demographic factors underlying disparities associated with foreign citizenship, to guide fair and inclusive adaptation strategies.

Additionally, this study's methodology provides a versatile framework for identifying vulnerability patterns across regions and scales, providing insights that can inform policies and interventions at the continental, national, and local levels.

## Data availability statement

The hazard and exposure data produced in this study (output of sections 2.2 and 2.3), the full database used as regression analysis input, and the estimated Eu-HVI values for the years 2000–2019 are available in CSV format, with report values for each NUTS2 region. It is possible to link the NUTS2 ID codes with their corresponding geometries from Eurostat to facilitate data visualization. Additionally, the Python scripts used for the hazard and exposure calculations and regression analysis are provided to ensure reproducibility.

The data that support the findings of this study are openly available at the following DOI: <https://doi.org/10.6084/m9.figshare.26413375>.

## Acknowledgments

We would like to thank the funding agencies for their support in this research. BS, LR, MM, and JCJHA were supported by the EU CLIMAAX Project (Grant No. 101093864). Additionally, JCJHA received support from the ERC Advanced Project COASTMOVE (Grant No. 884442). MM was also partly funded by the EU Project ICISK: Innovating Climate Services through Integrating Scientific and Local Knowledge (Grant Agreement No. 101037293). BS received partial funding from the European Union's Horizon 2020 research and innovation programme under the Project MYRIAD-EU (Grant Agreement No. 101003276).



## Appendix A

### A.1. Heatwave footprints

To calculate the footprints of the summer heatwaves, we implemented the following steps:

- 1) We selected  $T_{\text{air}}$  and  $T_{\text{dp}}$  data in the months June, July, and August between 2000 and 2019 from the ERA5 reanalysis [61], available at hourly intervals and in latitude-longitude grids of 0.25 degrees spatial resolution.
- 2) Using the calculated  $T_{\text{app}}$  (equation (1)) and the heatwave condition [51], we generated daily heatwave footprints as masked gridded layers. Each grid cell was assigned a numeric value if it satisfied the heatwave condition or was assigned a no data value if it did not. These footprints include: (a) the temperature parameter  $T_{\text{app-max}}$  and (b)  $N_{\text{days}}$ , a heatwave duration parameter.  $N_{\text{days}}$  assigns to each heatwave day the number of consecutive days from that day onward during which the heatwave condition remains valid. The value is highest on the start date of the heatwave event and decreases as the event progresses.
- 3) The daily gridded heatwave footprints were subsequently spatially aggregated at the regional NUTS2 level. For this, the regional temperature component  $T_{\text{app-max}}^{\text{NUTS2}}$  was computed as the average of all the  $T_{\text{app-max}}$  grid cell values whose centroid fell within the same NUTS2 region. The regional heatwave duration parameter  $N_{\text{days}}^{\text{NUTS2}}$  was determined as the average of the  $N_{\text{days}}$  across all the grid cells whose centroids fell within the same region.
- 4) We aggregated the NUTS2 daily values to a single value per heatwave event for inclusion in the regression analysis. We traced back from the fatalities report date in the temperature time series to identify the heatwave that preceded the reported fatalities. To achieve this, we filtered the database using the event dates provided in the fatalities dataset. For each NUTS2 region reported in the fatalities database, we identified the start date of the heatwave event as the day corresponding to the maximum  $N_{\text{days-max}}^{\text{NUTS2}}$  among the days leading up to the fatalities date. The end date of the event was determined as: start date +  $N_{\text{days-max}}^{\text{NUTS2}}$ .
- 5) To simplify the notation, the heatwave event duration parameter  $N_{\text{days-max}}^{\text{NUTS2}}$  was renamed  $N$ . The temperature parameter associated with the heatwave event was determined as the average of the  $T_{\text{app-max}}^{\text{NUTS2}}$  observed during the days of the

heatwave's duration and was called  $T$ .  $T$  and  $N$  served as the hazard variables in the regression analysis.

### A.2. Apparent temperature 90th percentile computation

To account for the climate warming trend, we calculated the daily apparent temperature percentiles of the monthly distributions separately for the decades 2000–2009 and 2010–2019, following standard recommendations to use 10 year windows for calculating temperature normals that reflect warming trends [96]. Figure A1 shows an overview of the 90th percentile of the daily apparent temperature for the months June, July and August of the decades 2000–2009 and 2010–2019 and their absolute difference between the two decades.

### A.3. LST

The LST data are processed following these steps: first, only the daytime records from the daily dataset are retained. For each heatwave day in the heatwave footprints dataset, regional averages of LST are computed across the entire duration of the heatwave. These LST values are then categorized into quartiles, and five categorical LST variables are created for use in the regression analysis: LST-Q1, LST-Q2, LST-Q3, LST-Q4, and LST-Missing. LST-Q1 is assigned a value of 1 for regions where the LST falls within the lowest quartile, and 0 otherwise, while LST-Q4 is assigned a value of 1 for regions within the highest quartile. The variable LST-Missing is assigned a value of 1 for cells where LST data are absent, either due to cloud cover or because the satellite's trajectory did not intersect that region on a given day. The interpretation of the regression results is based on the exclusion of LST-Q1, which serves as the baseline and is captured by the model constant. The coefficient for LST-Q2 reflects the effect on mortality associated with higher temperatures within the range defined by LST-Q2, compared to the temperature range of LST-Q1. Similarly, the coefficient for LST-Q3 indicates the effect on mortality of higher temperatures within the range of LST-Q3, relative to LST-Q1, and so on for the remaining dummy variables. The coefficient for LST-Missing does not have a direct interpretation; however, its inclusion ensures that all observations are used in the model, preventing the exclusion of cases with missing data from influencing the other explanatory variables.



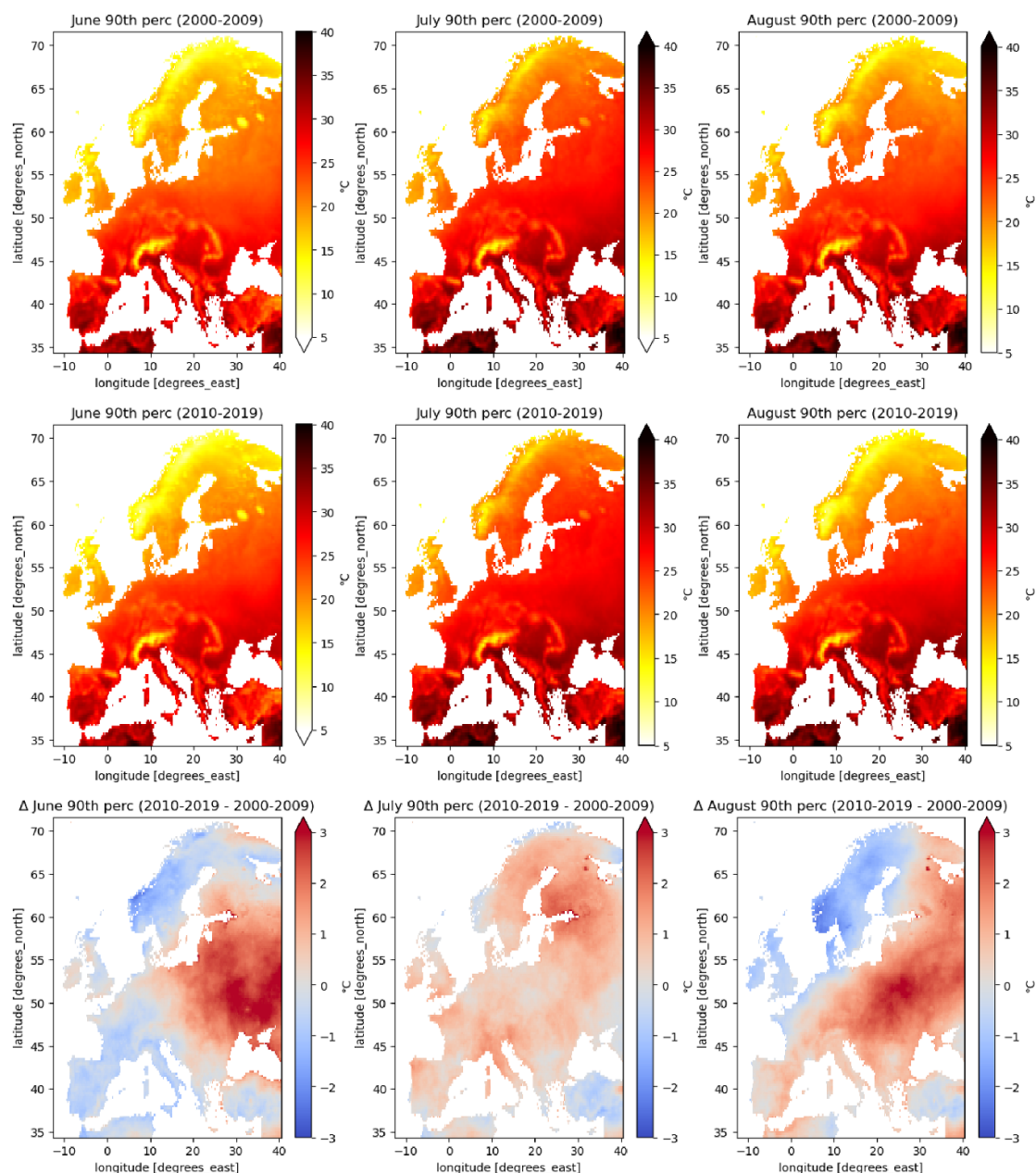


**Figure A1.** Hazard maps depicting the 90th percentile of apparent temperature ( $T_{app}$ ) for monthly distributions during the 2000–2009 (top) and 2010–2019 (mid) periods and their absolute difference (bottom).

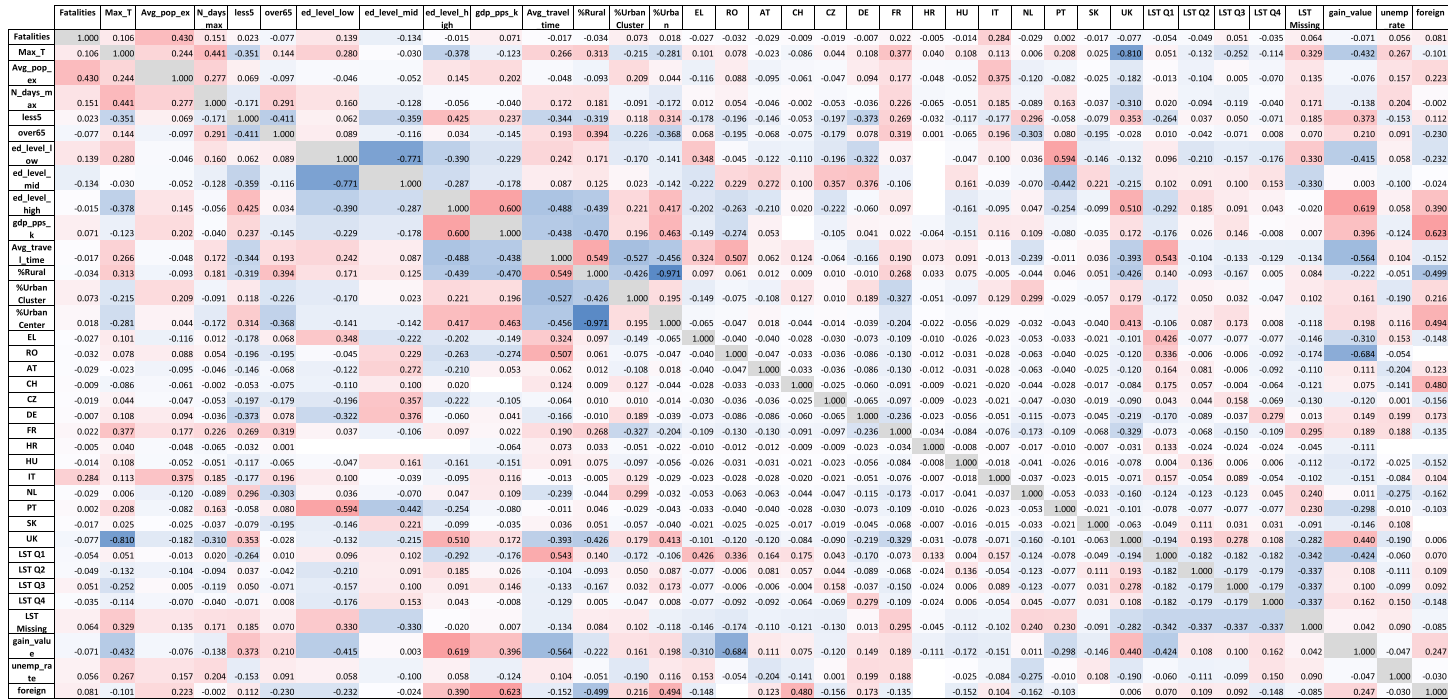
## Appendix B. Correlation matrices

	Fatalities	Max_T	Avg_pop_ex	%Urban Cluster	%Urban Center	EL	RO	AT	CH	CZ	DE	FR	HR	HU	IT	NL	PT	SK	UK	foreign
Fatalities	1.000	0.106	0.430	0.073	0.018	-0.027	-0.032	-0.029	-0.009	-0.019	-0.007	0.022	-0.005	-0.014	0.284	-0.029	0.002	-0.017	-0.077	0.081
Max_T	0.106	1.000	0.244	-0.215	-0.281	0.101	0.078	-0.023	-0.086	0.044	0.108	0.377	0.040	0.108	0.113	0.006	0.208	0.025	-0.810	-0.101
Avg_pop_ex	0.430	0.244	1.000	0.209	0.044	-0.116	0.088	-0.095	-0.061	-0.047	0.094	0.177	-0.048	-0.052	0.375	-0.120	-0.082	-0.025	-0.182	0.223
%Urban Cluster	0.073	-0.215	0.209	1.000	0.195	-0.149	-0.075	-0.108	0.127	0.010	0.189	-0.327	-0.051	-0.097	0.129	0.299	-0.029	-0.057	0.179	0.216
%Urban Center	0.018	-0.281	0.044	0.195	1.000	-0.065	-0.047	0.018	-0.044	-0.014	-0.039	-0.204	-0.022	-0.056	-0.029	-0.032	-0.043	-0.040	0.413	0.494
EL	-0.027	0.101	-0.116	-0.149	-0.065	1.000	-0.040	-0.040	-0.028	-0.030	-0.073	-0.109	-0.010	-0.026	-0.023	-0.053	-0.033	-0.021	-0.101	-0.148
RO	-0.032	0.078	0.088	-0.075	-0.047	-0.040	1.000	-0.047	-0.033	-0.036	-0.086	-0.130	-0.012	-0.031	-0.028	-0.063	-0.040	-0.025	-0.120	
AT	-0.029	-0.023	-0.095	-0.108	0.018	-0.040	-0.047	1.000	-0.033	-0.036	-0.086	-0.130	-0.012	-0.031	-0.028	-0.063	-0.040	-0.025	-0.120	0.123
CH	-0.009	-0.086	-0.061	0.127	-0.044	-0.028	-0.033	-0.033	1.000	-0.025	-0.060	-0.091	-0.009	-0.021	-0.020	-0.044	-0.028	-0.017	-0.084	0.480
CZ	-0.019	0.044	-0.047	0.010	-0.014	-0.030	-0.036	-0.036	-0.025	1.000	-0.065	-0.097	-0.009	-0.023	-0.021	-0.047	-0.030	-0.019	-0.090	-0.156
DE	-0.007	0.108	0.094	0.189	-0.039	-0.073	-0.086	-0.086	-0.060	-0.065	1.000	-0.236	-0.023	-0.056	-0.051	-0.115	-0.073	-0.045	-0.219	0.173
FR	0.022	0.377	0.177	-0.327	-0.204	-0.109	-0.130	-0.130	-0.091	-0.097	-0.236	1.000	-0.034	-0.084	-0.076	-0.173	-0.109	-0.068	-0.329	-0.135
HR	-0.005	0.040	-0.048	-0.051	-0.022	-0.010	-0.012	-0.012	-0.009	-0.009	-0.023	-0.034	1.000	-0.008	-0.007	-0.017	-0.010	-0.007	-0.031	
HU	-0.014	0.108	-0.052	-0.097	-0.056	-0.026	-0.031	-0.031	-0.021	-0.023	-0.056	-0.084	-0.008	1.000	-0.018	-0.041	-0.026	-0.016	-0.078	-0.152
IT	0.284	0.113	0.375	0.129	-0.029	-0.023	-0.028	-0.028	-0.020	-0.021	-0.051	-0.076	-0.007	-0.018	1.000	-0.037	-0.023	-0.015	-0.071	0.104
NL	-0.029	0.006	-0.120	0.299	-0.032	-0.053	-0.063	-0.063	-0.044	-0.047	-0.115	-0.173	-0.017	-0.041	-0.037	1.000	-0.053	-0.033	-0.160	-0.162
PT	0.002	0.208	-0.082	-0.029	-0.043	-0.033	-0.040	-0.040	-0.028	-0.030	-0.073	-0.109	-0.010	-0.026	-0.023	-0.053	1.000	-0.021	-0.101	-0.103
SK	-0.017	0.025	-0.025	-0.057	-0.040	-0.021	-0.025	-0.025	-0.017	-0.019	-0.045	-0.068	-0.007	-0.016	-0.015	-0.033	-0.021	1.000	-0.063	
UK	-0.077	-0.810	-0.182	0.179	0.413	-0.101	-0.120	-0.120	-0.084	-0.090	-0.219	-0.329	-0.031	-0.078	-0.071	-0.160	-0.101	-0.063	1.000	0.006
foreign	0.081	-0.101	0.223	0.216	0.494	-0.148		0.123	0.480	-0.156	0.173	-0.135		-0.152	0.104	-0.162	-0.103		0.006	1.000

Figure B1. Correlation matrix of the variables selected in the optimal models presented in table 2.

Table 3. VIF values for the models presented in table 2.

Variables	VIF Model 1 Baseline (H + E)	VIF Model 2 No country dummies (H + E + V)	VIF Model 3 Full flexibility (H+E+V+CD)
H: T (deg C)	1.855	3.291	—
E: Pop Exp (mln)	1.855	1.965	2.555
V: %Urban cluster (1–100)		2.483	4.043
%Urban center (1–100)		1.650	—
%Foreign citizens (1–100)		3.277	3.860
Country dummies (CD)			
AT			1.228
CH			1.746
CZ			1.061
DE			1.894
EL			1.011
FR			1.633
HU			1.008
IT			1.238
NL			1.624
PT			1.064
UK			2.074



### Appendix C. Additional model configurations considered

The following model configurations were evaluated but not selected as optimal due to their reduced statistical performance compared to the models presented in the Results section:

- **Model A:** a baseline model incorporating LST and exposure variables. This configuration yielded a lower adjusted  $R^2$  compared to Model 1.
- **Model B:** a variation of the best-fit Model 3, augmented with LST. This configuration exhibited multicollinearity among the variables, leading to unstable coefficient estimates that do not reliably isolate the individual effects of each predictor.
- **Model C:** a modification of the best-fit Model 3, substituting the country dummies with the ND-GAIN Adaptation Index. This model produced a substantially lower adjusted  $R^2$  than Model 3.
- **Model D:** an extension of Model C, with the inclusion of LST. The introduction of LST in this configuration also resulted in multicollinearity, reducing the robustness of the regression estimates.

**Table C1.** Examples of model configurations that result in reduced performance of the regression model respect to the optimal models presented in table 2.

Variables	Model A	Model B	Model C	Model D
<i>T</i> (deg C)				
LST Q1	−0.154 (0.294)	−0.024 (0.348) [VIF > 5]		0.328 (0.440) [VIF > 5]
LST Q2	0.504* (0.230)	0.256 (0.248) [VIF > 5]		1.242* (0.508) [VIF > 5]
LST Q3	0.176 (0.244)	−0.054 (0.227) [VIF > 5]		0.687 (0.509) [VIF > 5]
LST Q4	0.572* (0.247)	−0.033 (0.159) [VIF > 5]		1.638** (0.498) [VIF > 5]
LST missing	0.915*** (0.180)	−0.070 (0.181) [VIF > 5]		1.674*** (0.460) [VIF > 5]
<i>N</i> (days)				
Pop Exp (mln)	0.414*** (0.101)	0.295** (0.091)	0.303** (0.112)	0.267** (0.104)
Elderly % (1–100)				
Children % (1–100)				
GDP per inhabitant (kPPS)				
Education level 0–2% (1–100)				
Education level 3–4% (1–100)				
Education level 5–8% (1–100)				
% Unemployed (1–100)				
% Foreign citizens (1–100)		0.117*** (0.028)	0.089*** (0.019)	0.110*** (0.020)
ND-Gain adaptation index			−0.062 (0.038)	−0.081* (0.039)
Travel time to hospitals (min)				
% Rural (1–100)				
% Urban cluster (1–100)		0.073*** (0.018)	0.082*** (0.018)	0.074*** (0.018)
% Urban center (1–100)				
Country				
AT		0.512 (0.908)		
CH		0.890 (0.928)		
CZ		2.022* (0.961)		
DE		2.780** (0.828)		
EL		−0.088 (0.997)		
FR		2.070* (0.922)		
HU		3.770*** (0.962)		
IT		−3.514 (2.037)		
NL		2.697** (0.827)		
PT		2.505* (1.246)		
UK		−0.189 (0.846)		
Intercept	2.014*** (0.130)	0.075 (0.769)	5.673* (2.489)	5.570** (2.086)
N. Observations	278	251	251	251
Mean absolute error	1.440	0.727	1.367	1.288
Morans I	0.448**	0.345**	0.468**	0.444**
AIC	1109	791	977	963
Adjusted R <sup>2</sup>	0.172	0.659	0.246	0.299

## ORCID iDs

B Sestito  <https://orcid.org/0009-0002-3369-5040>

L Reimann  <https://orcid.org/0000-0002-9405-9147>

## References

- [1] van Daalen K R *et al* 2024 The 2024 Europe report of the *Lancet* Countdown on health and climate change: unprecedented warming demands unprecedented action *Lancet Public Health* **9** e495–522
- [2] Kenny G P, Poirier M P, Metsios G S, Boulay P, Dervis S, Friesen B J, Malcolm J, Sigal R J, Seely A J E and Flouris A D 2017 Hyperthermia and cardiovascular strain during an extreme heat exposure in young versus older adults *Temperature* **4** 79–88
- [3] Arsad F S, Hod R, Ahmad N, Ismail R, Mohamed N, Baharom M, Osman Y, Radi M F M and Tangang F 2022 The impact of heatwaves on mortality and morbidity and the associated vulnerability factors: a systematic review *Int. J. Environ. Res. Public Health* **19** 16356
- [4] Crandall C G and Wilson T E 2015 Human cardiovascular responses to passive heat stress *Compr. Physiol.* **5** 17
- [5] Ostro B D, Roth L A, Green R S and Basu R 2009 Estimating the mortality effect of the July 2006 California heat wave *Environ. Res.* **109** 614–9
- [6] Pascal M, Wagner V, Corso M, Laaidi K, Ung A and Beaudieu P 2018 Heat and cold related-mortality in 18 French cities *Environ. Int.* **121** 189–98
- [7] Alahmad B, Shakarchi A F, Khraishah H, Alseaidan M, Gasana J, Al-Hemoud A, Koutrakis P and Fox M A 2020 Extreme temperatures and mortality in Kuwait: who is vulnerable? *Sci. Total Environ.* **732** 139289
- [8] Ahmadnezhad E, Naieni K H, Ardalan A, Mahmoudi M, Yunesian M, Naddafi K and Mesdaghinia A R 2013 Excess mortality during heat waves, Tehran Iran: an ecological time-series study *J. Res. Health Sci.* **13** 24–31
- [9] Botzen W J W, Martinius M L, Bröde P, Folkerts M A, Ignjacevic P, Estrada F, Harmsen C N and Daanen H A M 2020 Economic valuation of climate change-induced



- mortality: age dependent cold and heat mortality in the Netherlands *Clim. Change* **162** 545–62
- [10] Stott P A, Stone D A and Allen M R 2004 Human contribution to the European heatwave of 2003 *Nature* **432** 610–4
  - [11] Pörtner H-O et al 2022 *IPCC 2022: Climate Change 2022: Impacts, Adaptation and Vulnerability: Working Group II Contribution to the Sixth Assessment Report of the Intergovernmental Panel on Climate Change* (Cambridge University Press)
  - [12] Fakhruddin B S H M, Boylan K, Wild A and Robertson R 2020 Assessing vulnerability and risk of climate change *Climate Extremes and Their Implications for Impact and Risk Assessment* (Elsevier) pp 217–41
  - [13] Stolte T R, Koks E E, de Moel H, Reimann L, van Vliet J, de Ruiter M C and Ward P J 2024 Vulnerability-drivers and dynamics of urban vulnerability based on a global systematic literature review *Int. J. Disaster Risk Reduct.* **108** 104535
  - [14] Li F, Yigitcanlar T, Nepal M, Thanh K N and Dur F 2022 Understanding urban heat vulnerability assessment methods: a PRISMA review *Energies* **15** 6998
  - [15] Rohat G, Flacke J, Dosio A, Pedde S, Dao H and van Maarseveen M 2019 Influence of changes in socioeconomic and climatic conditions on future heat-related health challenges in Europe *Glob. Planet. Change* **172** 45–59
  - [16] Dong J, Peng J, He X, Corcoran J, Qiu S and Wang X 2020 Heatwave-induced human health risk assessment in megacities based on heat stress-social vulnerability-human exposure framework *Landsc. Urban Plan.* **203** 103907
  - [17] Zhang L, Zhang Z, Ye T, Zhou M, Wang C, Yin P and Hou B 2018 Mortality effects of heat waves vary by age and area: a multi-area study in China *Environ. Health* **17** 1–12
  - [18] Soneja S, Jiang C, Fisher J, Upperman C R, Mitchell C and Sapkota A 2016 Exposure to extreme heat and precipitation events associated with increased risk of hospitalization for asthma in Maryland, USA *Environ. Health* **15** 1–7
  - [19] Smith C J 2019 Pediatric thermoregulation: considerations in the face of global climate change *Nutrients* **11** 2010
  - [20] Buscail C, Upegui E and Viel J-F 2012 Mapping heatwave health risk at the community level for public health action *Int. J. Health Geogr.* **11** 1–9
  - [21] Sera F et al 2020 Air conditioning and heat-related mortality: a multi-country longitudinal study *Epidemiology* **31** 779–87
  - [22] van Loenhout J A F and Guha-Sapir D 2016 How resilient is the general population to heatwaves? A knowledge survey from the enhance project in Brussels and Amsterdam *BMC Res. Notes* **9** 1–5
  - [23] van Loenhout J A F, Vanderplanken K, de Almeida M M, Kashibadze T, Giushvili N and Gamkrelidze A 2021 Heatwave preparedness in urban Georgia: a street survey in three cities *Sustain. Cities Soc.* **70** 102933
  - [24] Niu Y, Li Z, Gao Y, Liu X, Xu L, Vardoulakis S, Yue Y, Wang J and Liu Q 2021 A systematic review of the development and validation of the heat vulnerability index: major factors, methods and spatial units *Curr. Clim. Change Rep.* **7** 87–97
  - [25] Cutter S L, Boruff B J and Shirley W L 2012 Social vulnerability to environmental hazards *Hazards Vulnerability and Environmental Justice* (Routledge) pp 143–60
  - [26] Rizwan A M, Dennis L Y C and Liu C 2008 A review on the generation, determination and mitigation of urban heat island *J. Environ. Sci.* **20** 120–8
  - [27] Schlosberg D and Collins L B 2014 From environmental to climate justice: climate change and the discourse of environmental justice *Wiley Interdiscip. Rev. Clim. Change* **5** 359–74
  - [28] Burbidge M, Larsen T S, Feder S and Yan S 2022 Don't blame it on the sunshine! An exploration of the spatial distribution of heat injustice across districts in Antwerp, Belgium *Local Environ.* **27** 160–76
  - [29] Zeng P, Sun F, Shi D, Liu Y, Zhang R, Tian T and Che Y 2022 Integrating anthropogenic heat emissions and cooling accessibility to explore environmental justice in heat-related health risks in Shanghai, China *Landsc. Urban Plan.* **226** 104490
  - [30] Amado C 2022 Unravelling the Urban Heat Island phenomenon in the Netherlands. A multicity spatial analysis on the distributive component of environmental justice, analysing the urban green infrastructure, and the urban heat island effect *Master Thesis* Leiden University (<https://doi.org/10.2139/ssrn.4049664>)
  - [31] Mitchell B C, Chakraborty J and Basu P 2021 Social inequities in urban heat and greenspace: analyzing climate justice in Delhi, India *Int. J. Environ. Res. Public Health* **18** 4800
  - [32] Pappalardo S E, Zanetti C and Todeschi V 2023 Mapping urban heat islands and heat-related risk during heat waves from a climate justice perspective: a case study in the municipality of Padua (Italy) for inclusive adaptation policies *Landsc. Urban Plan.* **238** 104831
  - [33] Karner A, Hondula D M and Vanos J K 2015 Heat exposure during non-motorized travel: implications for transportation policy under climate change *J. Transp. Health* **2** 451–9
  - [34] Formetta G and Feyen L 2019 Empirical evidence of declining global vulnerability to climate-related hazards *Glob. Environ. Change* **57** 101920
  - [35] Jurgilevich A, Räsänen A, Groundstroem F and Juhola S 2017 A systematic review of dynamics in climate risk and vulnerability assessments *Environ. Res. Lett.* **12** 013002
  - [36] Wolf T, McGregor G and Analitis A 2014 Performance assessment of a heat wave vulnerability index for greater London, United Kingdom *Weather Clim. Soc.* **6** 32–46
  - [37] Grigorescu I, Mocanu I, Mitrică B, Dumitrașcu M, Dumitrică C and Dragotă C-S 2021 Socio-economic and environmental vulnerability to heat-related phenomena in Bucharest metropolitan area *Environ. Res.* **192** 110268
  - [38] Depietri Y, Welle T and Renaud F G 2013 Social vulnerability assessment of the Cologne urban area (Germany) to heat waves: links to ecosystem services *Int. J. Disaster Risk Reduct.* **6** 98–117
  - [39] Mashhoodi B 2021 Environmental justice and surface temperature: income, ethnic, gender and age inequalities *Sustain. Cities Soc.* **68** 102810
  - [40] Kim D-W, Deo R C, Lee J-S and Yeom J-M 2017 Mapping heatwave vulnerability in Korea *Nat. Hazards* **89** 35–55
  - [41] Chambers J 2020 Global and cross-country analysis of exposure of vulnerable populations to heatwaves from 1980 to 2018 *Clim. Change* **163** 539–58
  - [42] Rufat S, Tate E, Emrich C T and Antolini F 2019 How valid are social vulnerability models? *Ann. Am. Assoc. Geogr.* **109** 1131–53
  - [43] Reimann L, Koks E, de Moel H, Ton M J and Aerts J C J H 2024 An empirical social vulnerability map for flood risk assessment at global scale ("GlobE-SoVI") *Earth's Future* **12** e2023EF003895
  - [44] Burton C G 2010 Social vulnerability and hurricane impact modeling *Nat. Hazards Rev.* **11** 58–68
  - [45] Schmidtlein M C, Shafer J M, Berry M and Cutter S L 2011 Modeled earthquake losses and social vulnerability in Charleston, South Carolina *Appl. Geogr.* **31** 269–81
  - [46] Myers C A, Slack T and Singelmann J 2008 Social vulnerability and migration in the wake of disaster: the case of hurricanes Katrina and Rita *Popul. Environ.* **29** 271–91
  - [47] Reid C E et al 2012 Evaluation of a heat vulnerability index on abnormally hot days: an environmental public health tracking study *Environ. Health Perspect.* **120** 715–20
  - [48] Tate E 2012 Social vulnerability indices: a comparative assessment using uncertainty and sensitivity analysis *Nat. Hazards* **63** 325–47
  - [49] Joint Research Center (JRC) European Commission 2022 Disaster losses (available at: <http://data.europa.eu/89h/0030f450-6f4f-40c5-9390-66bb11dc2442>)

- [50] Belgium CRED/UCLouvain, Brussels 2023 EM-DAT The International Disaster Database (available at: [www.emdat.be](http://www.emdat.be))
- [51] D'Ippoliti D *et al* 2010 The impact of heat waves on mortality in 9 European cities: results from the EuroHEAT project *Environ. Health* **9** 1–9
- [52] Steadman R G 1979 The assessment of sultriness. Part I: a temperature-humidity index based on human physiology and clothing science *J. Appl. Meteorol. Climatol.* **18** 861–73
- [53] Harlan S L, Delet-Barreto J H, Stefanov W L and Petitti D B 2013 Neighborhood effects on heat deaths: social and environmental predictors of vulnerability in Maricopa County, Arizona *Environ. Health Perspect.* **121** 197–204
- [54] Goldblatt R, Addas A, Crull D, Maghrabi A, Levin G G and Rubinyi S 2021 Remotely sensed derived land surface temperature (LST) as a proxy for air temperature and thermal comfort at a small geographical scale *Land* **10** 410
- [55] Yang C, Yan F and Zhang S 2020 Comparison of land surface and air temperatures for quantifying summer and winter urban heat island in a snow climate city *J. Environ. Manage.* **265** 110563
- [56] Ghent D, Veal K and Perry M 2022 ESA Land Surface Temperature Climate Change Initiative (LST\_cci): multisensor Infra-Red (IR) Low Earth Orbit (LEO) land surface temperature (LST) time series level 3 supercollated (L3S) global product (1995–2020) (version 2.00) (<https://dx.doi.org/10.5285/ef8ce37b6af24469a2a4bdc31d3db27d>)
- [57] Schiavina M, Freire S and MacManus K 2022 GHS-POP R2022A—GHS Population Grid Multitemporal (1975–2030) (European Commission, Joint Research Centre)
- [58] Smith S K, Tayman J and Swanson D A 2013 *A Practitioner's Guide to State and Local Population Projections* (Springer)
- [59] Chen C, Noble I, Hellmann J, Coffee J, Murillo M and Chawla N 2015 *University of Notre Dame Global Adaptation Index* (University of Notre Dame)
- [60] Schiavina M, Melchiorri M and Pesaresi M 2023 GHS-SMOD R2023A—GHS Settlement Layers, Application of the Degree of Urbanisation Methodology (Stage I) to GHS-POP R2023A and GHS-BUILT-S R2023A, Multitemporal (1975–2030) vol 20 (European Commission, Joint Research Centre (JRC)) (<https://doi.org/10.2905/A0DF7A6F-49DE-46EA-9BDE-563437A6E2BA>)
- [61] Hersbach H *et al* 2020 The ERA5 global reanalysis *Q. J. R. Meteorol. Soc.* **146** 1999–2049
- [62] Eurostat 2024 Population on 1 January by broad age group, sex, and NUTS3 region ([https://doi.org/10.2908/DEMO\\_R\\_PJANAGGR3](https://doi.org/10.2908/DEMO_R_PJANAGGR3))
- [63] Eurostat 2024 Population on 1 January by age, sex and NUTS2 region ([https://doi.org/10.2908/DEMO\\_R\\_D2JAN](https://doi.org/10.2908/DEMO_R_D2JAN))
- [64] Eurostat 2024 Gross domestic product (GDP) at current market prices by NUTS3 regions ([https://doi.org/10.2908/NAMA\\_10R\\_3GDP](https://doi.org/10.2908/NAMA_10R_3GDP))
- [65] Office for National Statistics ONS 2022 Regional gross domestic product: all ITL regions (available at: [www.ons.gov.uk/economy/grossdomesticproductgdp/datasets/regionalgrossdomesticproductallnutslevelregions](http://www.ons.gov.uk/economy/grossdomesticproductgdp/datasets/regionalgrossdomesticproductallnutslevelregions))
- [66] Eurostat 2023 Population by educational attainment level, sex, and NUTS2 region (%) ([https://doi.org/10.2908/EDAT\\_LFSE\\_04](https://doi.org/10.2908/EDAT_LFSE_04))
- [67] Eurostat 2024 Population by sex, age, citizenship, labour status and NUTS2 region ([https://doi.org/10.2908/LFST\\_R\\_LFSD2PWN](https://doi.org/10.2908/LFST_R_LFSD2PWN))
- [68] Weiss D J *et al* 2020 Global maps of travel time to healthcare facilities *Nat. Med.* **26** 1835–8
- [69] Feng C, Wang H, Lu N, Chen T, He H, Lu Y and Tu X M 2014 Log-transformation and its implications for data analysis *Shanghai Arch. Psychiatry* **26** 105
- [70] Wooldridge J M 2013 *Introductory Econometrics: A Modern Approach* (South-Western Cengage Learning)
- [71] Furnival G M 1971 All possible regressions with less computation *Technometrics* **13** 403–8
- [72] Kim J H 2019 Multicollinearity and misleading statistical results *Korean J. Anesthesiol.* **72** 558
- [73] Cliff A and Ord K 1972 Testing for spatial autocorrelation among regression residuals *Geogr. Anal.* **4** 267–84
- [74] Nicholson D, Vanli O A, Jung S and Ozguven E E 2019 A spatial regression and clustering method for developing place-specific social vulnerability indices using census and social media data *Int. J. Disaster Risk Reduct.* **38** 101224
- [75] Qureshi A M and Rachid A 2022 Heat vulnerability index mapping: a case study of a medium-sized city (Amiens) *Climate* **10** 113
- [76] Calhoun Z D, Willard F, Ge C, Rodriguez C, Bergin M and Carlson D 2024 Estimating the effects of vegetation and increased albedo on the urban heat island effect with spatial causal inference *Sci. Rep.* **14** 540
- [77] Filho W L, Icaza L E, Neht A, Klavins M and Morgan E A 2018 Coping with the impacts of urban heat islands. A literature based study on understanding urban heat vulnerability and the need for resilience in cities in a global climate change context *J. Clean. Prod.* **171** 1140–9
- [78] Yin Y, He L, Wennberg P O and Frankenberg C 2023 Unequal exposure to heatwaves in Los Angeles: impact of uneven green spaces *Sci. Adv.* **9** eade8501
- [79] Hsu A, Sheriff G, Chakraborty T and Manya D 2021 Disproportionate exposure to urban heat island intensity across major US cities *Nat. Commun.* **12** 2721
- [80] Jiang L and O'Neill B C 2017 Global urbanization projections for the shared socioeconomic pathways *Glob. Environ. Change* **42** 193–9
- [81] Shaw B J, van Vliet J and Verborg P H 2020 The peri-urbanization of Europe: a systematic review of a multifaceted process *Landsc. Urban Plan.* **196** 103733
- [82] Berberian A G, Gonzalez D J X and Cushing L J 2022 Racial disparities in climate change-related health effects in the United States *Curr. Environ. Health Rep.* **9** 451–64
- [83] Madrigano J, Ito K, Johnson S, Kinney P L and Matte T 2015 A case-only study of vulnerability to heat wave-related mortality in New York City (2000–2011) *Environ. Health Perspect.* **123** 672–8
- [84] Reid C E, O'Neill M S, Gronlund C J, Brines S J, Brown D G, Diez-Roux A V and Schwartz J 2009 Mapping community determinants of heat vulnerability *Environ. Health Perspect.* **117** 1730–6
- [85] Taylor E V, Vaidyanathan A, Flanders W D, Murphy M, Spencer M and Noe R S 2018 Differences in heat-related mortality by citizenship status: United States, 2005–2014 *Am. J. Public Health* **108** S131–6
- [86] Santos D M D *et al* 2024 Twenty-first-century demographic and social inequalities of heat-related deaths in Brazilian urban areas *PLoS One* **19** e0295766
- [87] Alahmad B, Vicedo-Cabrera A M, Chen K, Garshick E, Bernstein A S, Schwartz J and Koutrakis P 2022 Climate change and health in Kuwait: temperature and mortality projections under different climatic scenarios *Environ. Res. Lett.* **17** 074001
- [88] Fong K C, Heo S, Lim C C, Kim H, Chan A, Lee W, Stewart R, Choi H M, Son J-Y and Bell M L 2022 The intersection of immigrant and environmental health: a scoping review of observational population exposure and epidemiologic studies *Environ. Health Perspect.* **130** 096001
- [89] Bogdanovich E, Brenning A, Reichstein M, De Polt K, Guenther L, Frank D and Orth R 2024 Official heat warnings miss situations with a detectable societal heat response in European countries *Int. J. Disaster Risk Reduct.* **100** 104206
- [90] Benmarhnia T, Deguen S, Kaufman J S and Smargiassi A 2015 Vulnerability to heat-related mortality: a systematic review, meta-analysis and meta-regression analysis *Epidemiology* **26** 781–93
- [91] de Luca C, Naumann S, Davis M and Tondelli S 2021 Nature-based solutions and sustainable urban planning in the European environmental policy framework: analysis of the state of the art and recommendations for future development *Sustainability* **13** 5021
- [92] Jay O *et al* 2021 Reducing the health effects of hot weather and heat extremes: from personal cooling strategies to green cities *Lancet* **398** 709–24

- [93] Fu J, Dupre K, Tavares S, King D and Banhalimi-Zakar Z 2022 Optimized greenery configuration to mitigate urban heat: a decade systematic review *Front. Archit. Res.* **11** 466–91
- [94] Doiron D *et al* 2024 Healthyplan.city: a web tool to support urban environmental equity and public health in Canadian communities *J. Urban Health* **101** 1–11
- [95] Ho H C, Knudby A and Huang W 2015 A spatial framework to map heat health risks at multiple scales *Int. J. Environ. Res. Public Health* **12** 16110–23
- [96] Arguez A and Vose R S 2011 The definition of the standard WMO climate normal: the key to deriving alternative climate normals *Bull. Am. Meteorol. Soc.* **92** 699–704